Est. 1984

ORIENTAL JOURNAL OF CHEMISTRY
An International Open Access, Peer Reviewed Research Journal

www.orientjchem.org

ISSN: 0970-020 X
CODEN: OJCHEG
2023, Vol. 39, No.(1):
Pg. 154-160

Synthesis and Antibacterial Study of Silver Nanoparticles-Nitrogen Doped Graphene Oxide-Chitosan Nanocomposite

ASMITHA BEEGUM. S[1]* and S. BEGILA DAVID[1]

[1]Department of Chemistry and Research Centre, Scott Christian College (Autonomous), Nagercoil-629 003, (Affiliated to Manonmaniam Sundaranar University, Abishekapatti, Tirunelveli-627 012, Tamilnadu, India.
*Corresponding author E-mail: asmithakalam@gmail.com

http://dx.doi.org/10.13005/ojc/390118

(Received: December 27, 2022; Accepted: February 20, 2022)

ABSTRACT

Herein, we report for the first time, the synthesis of silver nanoparticles-nitrogen doped graphene oxide-chitosan nanocomposite (SGC) from the aqueous leaf extract of *Curcuma caesia* plant and we explored bacterial toxicology behavior of SGC nanocomposite via agar disc diffusion method. *Curcuma caesia* is a medicinal herb utilized as a reducing agent for the reduction of silver-to-silver ions. Graphene oxide is a significant two-dimensional carbon nanomaterial, possessing excellent physical, chemical, and electrical properties that make them unique for various applications. The Ultrasonication process at room temperature was utilized for the synthesis of SGC nanocomposite. The addition of biopolymer; chitosan, and silver nanoparticles (AgNPs) to the matrix of nitrogen-doped graphene oxide (NGO) was confirmed via various spectroscopic techniques such as FTIR, FT-Raman, XPS, and so on. Finally, the results of the disc diffusion method showed SGC nanocomposite exhibit concentration-dependent inhibition toward bacterial growth.

Keywords: *Curcuma caesia*, Silver nanoparticles, FT-Raman, Chitosan, Melamine, Antibacterial activity.

INTRODUCTION

Graphene (GR) forms a basic structure of graphene-based materials, a honeycomb lattice with sp^2 bonded carbon in a two-dimensional array, having excellent physical and electronic properties. Graphene oxide (GO) is derivative of GR. It is the oxidized form bearing a 2D plane with an abundance of oxygen functionalities such as epoxy, hydroxyl, and carboxylic groups which provide a reactive site for the nucleation and binding of various metal nanoparticles, and for that reason, graphene oxide is suitable in biomedical applications[1]. Many nanoparticles have already been dispersed and stabilized using GO nanosheets as supports (Au, TiO_2, ZnO, Fe_3O_4)[2,3]. Graphene oxide surface enriched with oxygen functionalities mold them for interactivity with other metal nanoparticles such as silver, gold, etc. via physisorption, electrostatic binding, or charge-transfer interactions[4]. Understanding the relation between graphene nanomaterials and other nanomaterials provides a new direction for the

fabrication of other efficient graphene nanomaterial-based composites. Chitosan (CTS), the foremost cost-effective, innocuous, biocompatible, and most amazing raw biomaterial derived from chitin, a polysaccharide found in crustaceans via the deacetylation process. The excellent physical properties like antimicrobial, nontoxicity, high biocompatibility, and bio-absorbability make them a good candidate for various applications including the food, pharmaceutical, and environmental industries. The amino group NH_2 at the C-2 position of chitosan is responsible for its outstanding chemical behavior, whose solubility in diluted acidic aqueous solutions gets improved on protonation, offering a unique opportunity to serve various biomedical applications. The intriguing properties of chitosan, together with its capacity to be processed in various structures and mixed with various nanomaterials, result in a wide range of applications, including drug delivery, tissue regeneration, and biosensing[5]. Cross-linking GO sheets with biopolymers as cross-linkers via noncovalent or covalent bonding can result in GO framework topologies[6,7]. Chitosan (CTS) is one of a series of abundant renewable biopolymers[8] that has been used as an adsorbent for the removal of organic dyes from aqueous solution[9] due to the presence of active adsorption sites (hydroxyl and amino groups). CTS may be amidated with GO carboxyl groups to form a homogenous, well-dispersed GO composite[10,11]. In multiple recent studies, silver nanoparticles (AgNPs) have been added to GO/CS systems to give the nanocomposite additional antibacterial characteristics[12,13].

The present work aimed at the synthesis and characterization of silver nanoparticle-nitrogen doped graphene oxide-chitosan nanocomposite (SGC) via biosynthesis using *Curcuma caesia* leaf extract as a novel, cost-effective, eco-friendly reducing agent and explored its bacterial toxicology behavior. *Curcuma caesia* roxb. belongs to the family zingiberaceae, commonly called black turmeric or black zedoary. The polyphenols and flavonoids present are the sources of the reduction process[14]. Based on the foregoing considerations, one of the principal goals of this research was to design a simple method for preparing a silver nanoparticles-nitrogen doped graphene oxide-chitosan nanocomposite by cross-linking NGO-AgNPs with CTS to obtain a material with enhanced physicochemical properties for a variety of applications. The structural and compositional analysis of SGC nanocomposite was achieved via FTIR, Raman spectroscopy, and XPS analysis. The data regarding the thermal stability and surface morphology of the SGC nanocomposites were investigated using thermogravimetric analysis (TGA) and transmission electron microscopy (TEM). The antibacterial activity was studied using the agar disc diffusion method against eight bacterial strains such as *Staphylococcus aureus, Streptococcus aureus, Enterococcus faecalis, Bacillus cereus, Klebsiella pneumoniae, Proteus mirabilis, E. coli, Pseudomonas aeruginosa*. This is for the first time, we report research on the synthesis, characterization, and antibacterial properties of synthesized SGC which is prepared by using *Curcuma caesia* leaf extract.

EXPERIMENTAL

Materials

Graphite powder (100 mesh, 99.9%,), sulfuric acid (H_2SO_4, 98%), phosphoric acid (H_3PO_4), Hydrogen peroxide (H_2O_2, 30%), Chitosan (>75% deacetylated), Melamine ($C_3H_6N_6$) were purchased from Sigma-Aldrich, India. Sodium nitrate ($NaNO_3$), Potassium permanganate, ($KMnO_4$), Hydrogen chloride (HCl), Silver nitrate ($AgNO_3$), and double distilled water are collected from respective suppliers. Muller Hinton Agar Medium (HI Media) and *Curcuma caesia* leaves were bought from Lingam Gardens, Chennai.

METHODS

Preparation of Curcuma Caesia leaf Extract

The leaves of *Curcuma caesia* leaf extract were collected from Lingam Gardens, Chennai. The leaves were washed with deionized water several times and later cut into small pieces and shaded dry for two weeks, then converted into fine powder. The weight of *Curcuma caesia* leaf powder was 20 g. This powder was dissolved in 100 mL of distilled water and boiled for 5 min at 100°C, a color change of greenish yellow was observed. The extract was filtered with the Whatman No.1 filter Paper. Then the filtrate was stored in a tight seal pack under 4°C for further use.

Preparation of silver nanoparticles-nitrogen-doped graphene oxide-chitosan nanocomposite

Nitrogen-doped graphene oxide was

prepared from graphite powder via a one-pot modified Hummer's method using melamine as a nitrogen precursor. Graphite powder (0.25 g) was added to the mixture of acid [H_2SO_4 & H_3PO_4] at 0-5^{0}C. Then, $KMnO_4$ was slowly added on constant stirring for about 30 minutes. The mixture was then kept at 30-35^{0}C and stirred continuously for 20 h to form GO sheets. Thereafter, a particular amount of melamine was introduced to the mixture and continued stirring for 22 hours. Finally, the chemical reaction was ceased by the addition of distilled water followed by the subsequent addition of H_2O_2. The impurities were washed off with 10% HCl and the centrifugation was continued till the pH become neutral. The obtained brown precipitate was dried to yield nitrogen-doped graphene oxide. The aqueous solution of nitrogen-doped graphene oxide (NGO) was ultrasonicated with 25 mL of *Curcuma caesia* leaf extract for about 15 mins followed by gradual addition of $AgNO_3$ solution (10Mm) under vigorous stirring for about 24 h at 30^{0}C. Finally, washed and dried in the hot-air oven to obtain silver nanoparticle-nitrogen-doped graphene oxide (SNGO). The obtained powder of SNGO was dissolved in 50 mL of deionized water and sonicated for about 45 min to obtain a homogenous suspension. Then added a mixture of chitosan solution (1:1 chitosan: glacial acetic acid) and ultrasonicated for 30 mins at a frequency of 25 kHz. To cause the precipitation of material 20 mL NaOH was added and kept in the mixture for another 30 mins followed by washing with distilled water and drying at room temperature to obtain the nanocomposite (SGC).

Bacterial toxicology evaluation

To investigate the prelude antibacterial behavior of the synthesized polymer nanocomposite SGC, eight bacterial strains were selected that cause food-borne illnesses such as *Gram-negative* bacterial species (*Pseudomonas aeruginosa, Klebsiella pneumoniae, Proteus mirabilis,* and *E. coli*) and *Gram-positive* species (*Staphylococcus aureus, streptococcus aureus, Enterococcus faecalis*, and *Bacillus cereus*) strains. The antibacterial analysis carries out in view of the diameter of the inhibition zone. The antibacterial potential of synthesized nanocomposite was investigated using the agar disc diffusion method. The bacterial strains were grown on Muller Hinton Agar medium at 37^{0}C for 24 hours. Then the pathogenic bacterial strains were swabbed onto the plates. Afterward, the SGC sample of different concentrates (2.5 mg, 5 mg, 7.5 mg, 10 mg/mL) was loaded onto the disc along with standard antibiotic streptomycin as positive control and then placed on the surface of Muller Hinton Medium, and plates were incubated at 37^{0}C for 24 hours. The diameter of the zone of inhibition was measured using an accurate digital ruler in mm. The absence of a zone of inhibition was interpreted as the absence of activity.

RESULTS AND DISCUSSION

FTIR analysis

FTIR spectrum of NGO shown in Fig. 1 confirms the doping of nitrogen atoms into the lattice of graphene oxide, in addition, the spectrum explains the presence of other oxygen functionalities such as hydroxyl, carbonyl, epoxy, and so on[15]. A strong broad peak around 3402 cm^{-1} shows the presence of O-H or N-H group in NGO. and a peak at 1722 cm^{-1} was attributed to the carbonyl (C=O) stretching. The peaks at 1046 cm^{-1} and 1623 cm^{-1} confirm the existence of epoxy C-O stretching and C=C stretching vibrations, respectively. Furthermore, the nitrogen doping was validated by the presence of C=N and C-N groups at stretching vibrations of 1320 cm^{-1} and 1402 cm^{-1} respectively[16]. There observed an increase in the intensity of the C=C group due to the addition of silver nanoparticles shows the interactivity between NGO and AgNPs, which is further supported by previous reports[17]. Finally, FTIR spectra of SGC in Fig. 1 showed a combination of characteristic peaks of SNGO and Chitosan. The interaction between three components ie, NGO, silver ions, and chitosan was disclosed by a change in intensity. The broad and strong peak at 3404 cm^{-1} shows N-H/O-H stretching vibration from NGO or chitosan or AgNPs, and a peak at 1724 cm^{-1} was absent here. The vibrational mode of amide C=O stretching was shown by peaks at 1640 cm^{-1} and 1578 cm^{-1} attributed to amide moiety which indicated the presence of amide linkage that confirms the bonding between chitosan molecule and SNGO material. Thus, the FTIR data substantiate the formation of SGC nanocomposite.

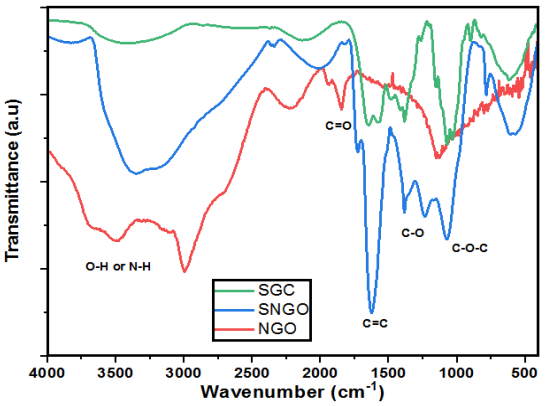

Fig. 1. FT-IR spectra of NGO, SNGO and SGC

FT-raman analysis

The Raman spectra of NGO nanomaterial consist of a prominent G-band at 1588 cm^{-1} representing the planar configuration Sp^2 bonded carbon, and a D-band at 1347 cm^{-1} attributed to disorder induction[18]. Raman spectra of NGO are shown in Fig. 2a, the ID/IG ratio of NGO is 0.82, where the rise in the intensity ratio suggests an increase in defects and disorder occurred during the doping process due to the inclusion of N atoms into the Sp^2 carbon skeleton of GO. We witnessed an increase in ID/IG ratio of NGO due to the introduction of AgNPs which clearly depicts the expansion in the degree of disorder, also the color of the AgNPs/NGO (SNGO) composite sheets progressively changes to coffee brown; this might also be a result of the nanoparticles' plasmon absorption shown in Fig. 2b. The Raman spectra of SGC Fig. 2c, consists of two bands G band at 1586 cm^{-1} and D band at 1349 cm^{-1} respectively with an increase in intensity. The ID/IG ratio of the SGC nanocomposite got enhanced (0.87) as compared to NGO (0.82) which means that the Sp^3 carbon domain was increased with the functionalization of GO by a biopolymer.

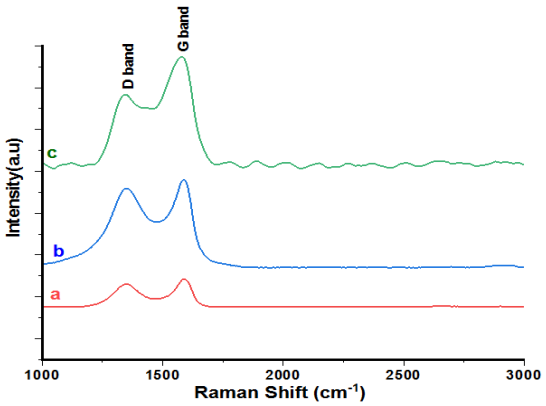

Fig. 2. FT-raman spectrum of a) NGO, b) SNGO and c) SGC

XPS analysis

The surface chemistry of SGC nanocomposite was distinguished using X-ray photoelectron spectroscopy (XPS). The XPS peak survey of NGO, SNGO & SGC is shown in Fig. 3a, NGO exhibited distinctive C1s peak (284.8 eV), N1s peak (398.6 eV and O1s peak (531.2eV) shown in Fig. 3A. The amount of nitrogen incorporated in the NGO was found to be 5.5 at%. The reduction in oxygen levels was observed (33.68% to 32.86%) shown in Table 1 suggesting substitution by N groups. As expected, the XPS peaks for each element C, N, Ag, and O were all present in the XPS survey of SNGO. C1s is around 284.2 eV, N1s at 397.1 eV, O1s at 530.9 eV, and a doublet of Ag3d was observed at 366.1 and 372.16 eV shown in Fig. 3b, which arise from spin-orbit coupling (3d5/2 and 3d3/2). The nitrogen-to-carbon atomic ratio found as 0.08 and Ag to C ratio decreased (~ 0.05) for SNGO due to the agglomeration of Ag. As compared to NGO and SNGO, the deconvolution of C1s spectra showed a remarkable drop in intensity for C-O and C=O and a rise in intensity for C=C species in the SGC nanocomposite. The deconvolution of C1s displayed an additional peak around 287.02 eV which was attributed to N-C=O shown in Fig. 3c which is absent for NGO and SNGO samples and the data supports the conclusion that chitosan in the SGC nanohybrids was successfully bound to the surface of the N-doped graphene oxide nanosheets.

TEM analysis

The TEM micrograph of NGO Fig. 4a showed a flaky, smooth, and paper-like structure having a wrinkled morphology with a grain size of 0.26nm[19]. This morphology is due to the stimulation of defects that were introduced during the doping process. The TEM image of SNGO, Fig. 4b illustrates some amount of aggregation of AgNPs with an average size of approximately 30nm with spherical geometry having a grain size of 0.21nm. These agree with the XRD results, which suggest the FCC pattern of AgNPs. In the final product, Fig. 4c the AgNPs appear to be more agglomerated with distorted spherical geometry and have a larger particle size (mean particle size ~47nm). Furthermore, the zeta potential measurement showed that the NGO surface has a negative zeta potential of –20.5mV, which shifted to a positive zeta value of (+39.8 mV) upon the addition of biopolymer resulting from the protonation of amino groups $(NH_3)^+$ of chitosan

polymeric layer. Hence, it possesses high stability. The SAED Fig. 4d pattern shows the synthesized SGC material is crystalline.

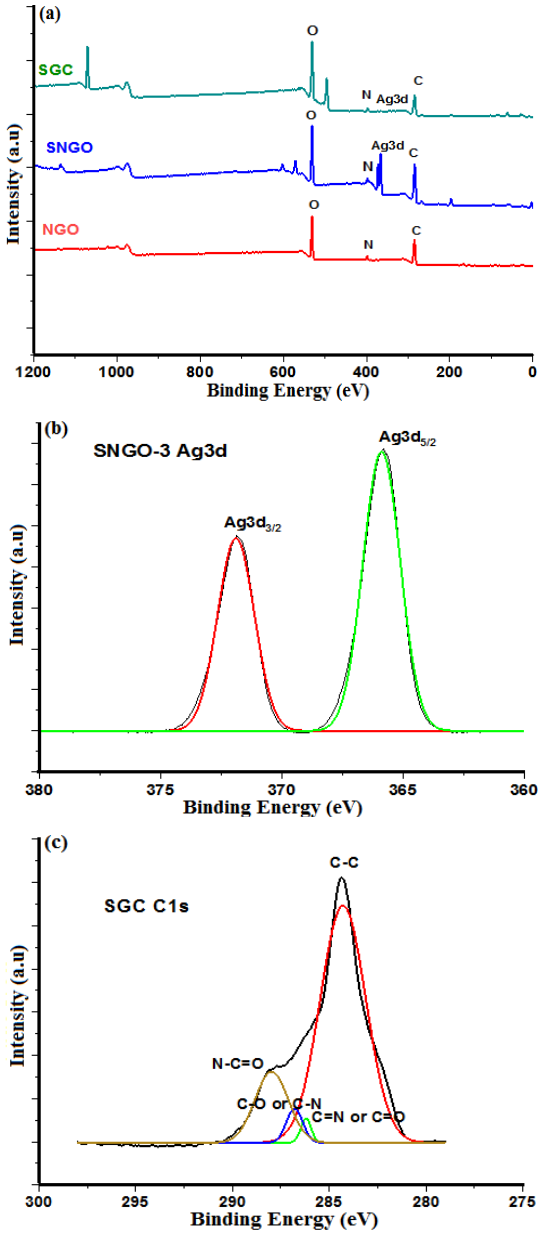

Fig. 3a. XPS spectrum of NGO, SNGO, and SGC, b) Ag3d of SNGO and c) C1s of SGC

Table 1: Atomic content of C, N, O, and Ag in synthesized nanocomposite

Sample	Elemental composition %			
	C	O	N	Ag
NGO	61.7	32.86	5.44	-
SNGO	62.07	28.89	5.43	3.51
SGC	48.88	46.91	4.21	0.07

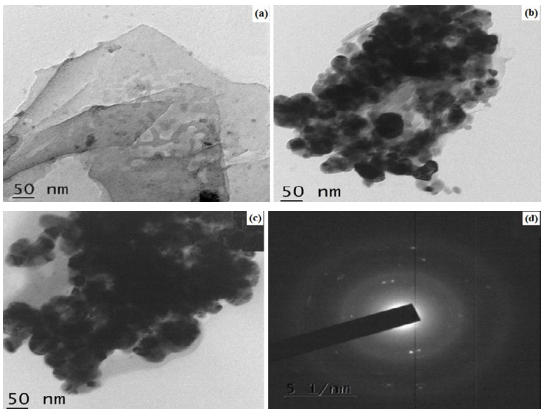

Fig. 4. TEM images of a) NGO, b) SNGO, and c) & d) TEM image and SAED of SGC respectively

TGA analysis

The thermal stability of NGO and SGC nanocomposite was investigated by TGA analysis. The TGA curves of NGO and SGC are shown in Fig. 5a and 5b respectively. NGO showed two steps of decomposition. The initial weight loss for the NGO was noticed below 100°C corresponding to the loss of water molecules. The major weight loss of NGO was observed in the range of 120-220°C which can be attributed to the removal of most of the oxygen-containing functional groups. At a higher temperature around 550°C, the weight loss was attributed to the decomposition of the carbon skeleton. This demonstrated its excellent thermal stability[20]. In SGC, they showed three-step decomposition stages, chitosan branches could increase the thermal stability of NGO as the sharp weight loss was delayed. The presence of both AgNPs and NGO increased the Tg of the SGC composite to 274.4°C, which is higher as compared to a bare NGO as well as a biopolymer. The increase in Tg is ascribed to the interaction between CS chains and NGO sheets and AgNPs. Through hydrogen bonding and electrostatic contact, such interaction may restrict the segmental motion of CS chains, increasing their thermal stability.

Antibacterial assessment

The antibacterial potential of silver nanoparticles-nitrogen-doped graphene oxide-chitosan nanocomposite was investigated by eight typical food pathogenic microbes

Gram-positive (*Staphylococcus* sps, *Streptococcus* sps, *Enterococcus* sps, *Bacillus* sps) and *Gram-negative* (*E. coli, Pseudomonas* sps, *Klebsiella* sps, *Proteus* sps) which usually found in the surface of vegetables and fruits. The antibacterial potential was determined by the size of the inhibition zone which is assessed against eight bacterial strains, along with streptomycin as control. The SGC did not show any remarkable activity against the tested bacterial strain at a concentration of 2.5 mg/mL. Instead, the nanocomposite exhibited excellent antibacterial activity against three strains (*Staphylococcus* sps, *Enterococcus* sps, and *Klebsiella* sps) at a concentration of 7.5 mg/mL and above. The SGC showed an enhanced inhibition zone than positive control for *Enterococcus* and *Klebsiella* species in Table 2. Therefore, we can conclude that the SGC nanocomposite could be used as an antibacterial agent with concentration-dependent applications. Fig. 6 depicts the antibacterial activity of SGC nanocomposite and the zone of inhibition given in Table 2.

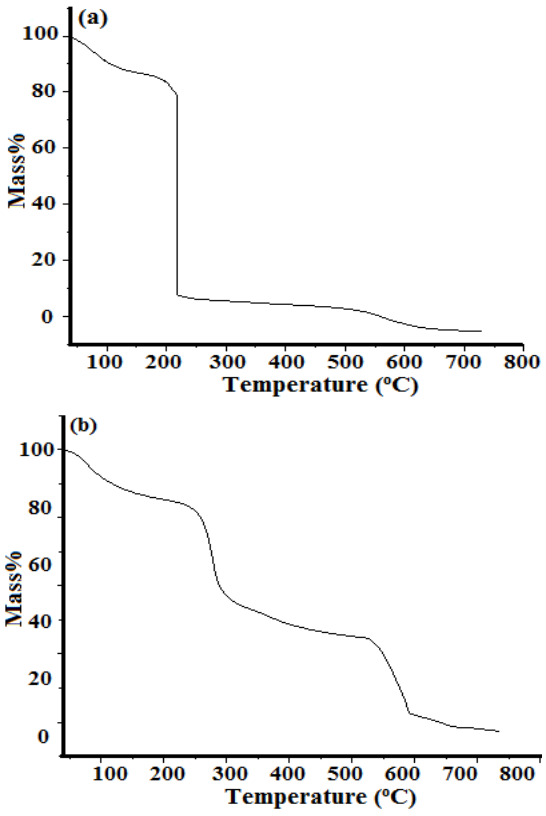

Fig. 5. TGA curves of a) NGO and b) SGC

Table 2: Antibacterial potential of SGC

Bacteria Name	Zone of inhibition (mm in diameter)					
	SGC					PC
	2.5mg	5mg	7.5mg	10mg		25mg
Staphylococcus aureus	-	-	8mm	9mm		11mm
Streptococcus aureus	-	-	-	-		19mm
Enterococcus faecalis	-	10mm	13mm	26mm		22mm
Bacillus cereus	-	-	-	-		11mm
Klebsiella pneumoniae	-	-	13mm	17mm		13mm
Proteus mirabilis	-	-	-	-		23mm
E. coli	-	-	-	-		15mm
Pseudomonas aeruginosa	-	-	-	-		11mm

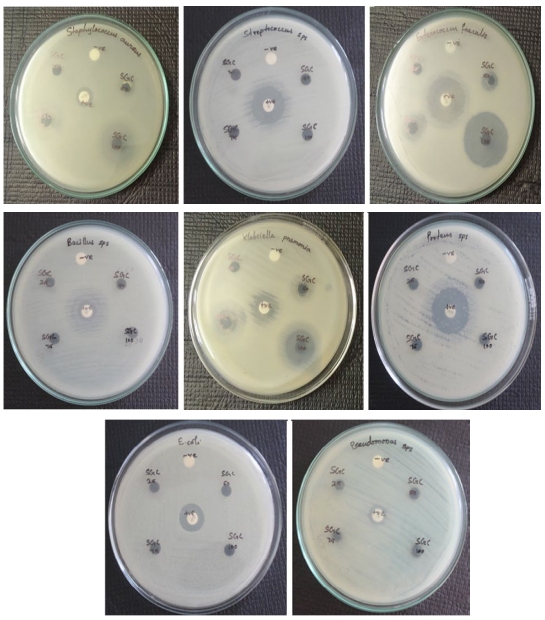

Fig. 6. Antibacterial activity of SGC nanocomposite

CONCLUSION

A low-temperature, green route was employed to synthesize silver nanoparticle-nitrogen-doped graphene oxide-chitosan nanocomposite. Various spectroscopic analyses confirmed the

successful formation of the nanocomposite. In addition to oxygen functionalities, the FTIR confirms the presence of an N atom on the GO framework and impregnation of silver nanoparticles and chitosan to NGO surface. Raman spectrum confirmed the inclusion of nitrogen atoms, silver, and biopolymer, chitosan into the GO surface via a change in ID/IG ratio of SGC which is around 0.87. The TEM showed that SGC has a crystalline structure and excellent thermal stability. Also, investigated their antibacterial activity against some selected food pathogenic microbes using an agar disc diffusion method. From the results, we concluded that the SGC nanocomposite exhibit concentration-dependent inhibition towards bacterial growth, they are active at a concentration of 7.5 mg/mL and above thus, reveal excellent activity towards three strains: *Staphylococcus aureus*, *Klebsiella pneumoniae*, and *Enterococcus faecalis*. Hence, the synthesized SGC nanocomposite can be used for various applications including the biomedical, food industry, and so on.

ACKNOWLEDGEMENT

The authors would like to thank STIC Cochin, Kerala for instrumental support.

Conflict of interest

The authors declare no conflict of interest

REFERENCES

1. Tiwari, H.; Karki, N.; Pal, M.; Basak, S.; Verma, R.K.; Bal, R.; Kandpal, N.D.; Bisht, G.; Sahoo, N.G. *Colloids Surf. B, Biointerfaces*., **2019**, *178*, 452–459.
2. J. J. Liang, Y. F. Xu, D. Sui, L. Zhang, Y. Huang, Y. F. Ma, F. F. Li, Y. S. Chen, *J. Phys. Chem*., **2010**, *114*, 17465.
3. X. Q. Fu, F. L. Bei, X. Wang, S. O'Brien, J. R. Lombardi, *Nanoscale*., **2010**, *2*, 1461.
4. Hui, K. S.; Hui, K. N.; Dinh, D. A.; Tsang, C. H.; Cho, Y. R.; Zhou, W.; Hong, X.; Chun, H. H. *Acta Mater*., **2014**, *64*, 326–332.
5. Rinaudo, M. *Polym Int*., **2008**, *57*, 397–430.
6. Park, S.; Lee, K.-S.; Bozoklu, G.; Cai, W.; Nguyen, S. T.; Ruoff, R. S. *ACS Nano*., **2008**, *2*, 572–578.
7. Turgut, H.; Tian, Z. R.; Yu, F.; Zhou, W. *J. Phys. Chem*. C., **2017**, *121*, 5829–5835.
8. Duri, S.; Tran, C. D. *Langmuir*., **2013**, *29*, 5037–5049.
9. Wu, F. C.; Tseng, R. L.; Juang, R. S. *Water Res*., **2001**, *35*, 613–618.
10. Yang, X.; Tu, Y.; Li, L.; Shang, S.; Tao, X.M. *ACS Appl. Mater. Interfaces*., **2010**, *2*, 1707–1713.
11. Chen, Y.; Chen, L.; Bai, H.; Li, L. *J. Mater. Chem. A*., **2013**, *1*, 1992–2001.
12. Khawaja, H.; Zahir E.; Asghar, M.A.; Asghar, M.A. *Colloids Surf. A Physicochem. Eng. Asp*., **2018**, *555*, 246–255.
13. Keshvardoostchokami, M.; Piri, F.; Jafarian, V.; Zamani A. *JOM*., **2020**, *72*, 4477–4485.
14. Angana, B.; Manabi, P.; Roktim, G.; Loying, R.; Sarma, N.; Sunita, M.; Pandey, S.K.; Lal, M. *Industrial Crops & Products*., **2019**, *129*, 448–454.
15. Karolina Ollika.; Maria Rybarczyk.; Jakub Karczewski.; Marek Lieder. *Applied Surface Science*., **2020**, *499*, ID 143914.
16. Li, Y.; Pan, D.; Zhang, M.; Xie, J; and Yan, Z. *RSC Advances*., **2016**, *6*(54), 48357–48364.
17. Mo Z.Y.; Zheng R.P.; Peng H.L.; Liang H.G. *J Power Sources*., **2014**, *245*, 801-807.
18. Ferrari, A.C.; Robertson, *J. Phys. Rev. B*., **2002**, *61*, 14095-14107.
19. Alsaiari, N.S.; Abdelfattah, A.; Khadijah, M.K.; Alzahrani, F.M.; Faouzi, B.R.; Mohamed, A.T. *Adsorption Science & Technology*., **2022**, *14*, ID 9417542.
20. Yokwana, K.; Sekhar C. R.; Mohammad K.F.; Alex T. K.; Bhekie B. M.; Sabelo D. M.; Edward N. N. *J. Nano Sci. Nanotechnol*., **2018**, *18*, 5470-5484.